Robust analysis of the growth of structure

Deng Wang[*] and Olga Mena[†]

Instituto de Física Corpuscular (CSIC-Universitat de València), E-46980 Paterna, Spain

(Received 11 December 2023; accepted 28 March 2024; published 30 April 2024)

Current cosmological tensions show that it is crucial to test the predictions from the canonical ΛCDM paradigm at different cosmic times. One very appealing test of structure formation in the Universe is the growth rate of structure in our universe f, usually parametrized via the growth index γ, with $f \equiv \Omega_m(a)^\gamma$ and $\gamma \simeq 0.55$ in the standard ΛCDM case. Recent studies have claimed a suppression of the growth of structure from a variety of cosmological observations, characterized by $\gamma > 0.55$. By employing different self-consistent growth parametrizations schemes, we show here that $\gamma < 0.55$, obtaining instead *an enhanced growth of structure today.* This preference reaches the 3σ significance using cosmic microwave background observations, supernova Ia and baryon acoustic oscillation measurements. The addition of cosmic microwave background lensing data relaxes such a preference to the 2σ level, since a larger lensing effect can always be compensated with a smaller structure growth, or, equivalently, with $\gamma > 0.55$. We have also included the lensing amplitude $A_{\rm L}$ as a free parameter in our data analysis, showing that the preference for $A_{\rm L} > 1$ still remains, except for some particular parametrizations when lensing observations are included. We also do not find any significant preference for an oscillatory dependence of $A_{\rm L}$, $A_{\rm L} + A_m \sin \ell$. To further reassess the effects of a nonstandard growth, we have computed by means of N-body simulations the dark matter density fields, the dark matter halo mass functions and the halo density profiles for different values of γ. Future observations from the Square Kilometer Array, reducing by a factor of 3 the current errors on the γ parameter, further confirm or refute with a strong statistical significance the deviation of the growth index from its standard value.

DOI: 10.1103/PhysRevD.109.083539

I. INTRODUCTION

Cosmological observations can be optimally fitted within the minimal ΛCDM model, described by six fundamental parameters. This model has successfully explained a large number of measurements at different scales. Nevertheless, there are a number of tensions. The Hubble constant one [1] is the most significant tension (5σ), and it implies the mismatching between the value of the Hubble constant obtained from Planck-2018 CMB observations ($H_0 = 67.4 \pm 0.5$ km s^{-1} Mpc^{-1} [2]) and the value of H_0 from local measurements using SNIa calibrated with Cepheid variable stars ($H_0 = 73 \pm 1$ km s^{-1} Mpc^{-1} [3]). Other measurements, such as the tip of the red giant branch (TRGB) method, one of the most precise and accurate means of measuring distances in the local universe, provides $H_0 = 69.6 \pm 1.9$ km s^{-1} Mpc^{-1} [4,5], while time-delay measurements of strong gravitational lensing provides measurements of the Hubble constant consistent with both Cepheids and CMB/TRGB observations [6,7], due to the modeling of the lens mass distribution.

A second conundrum, even if less significant, is the S_8 tension, a parameter closely related to the matter clustering of matter in the Universe. S_8 could be inferred from the measurements of CMB anisotropies as those from Planck, and, more directly, from the measurements of galaxy lensing made by large surveys such as the Dark Energy Survey (DES) [8–10], and the Kilo-Degree Survey (KiDS) [11–13]. While Planck CMB data favors a larger value of S_8, galaxy surveys (the DES [8–10] and the KiDS-1000 surveys [11–13]) prefer a lower one, leading to a $2 \sim 3\sigma$ discrepancy and indicating a possible redshift evolution of S_8 (see Ref. [14]). Nevertheless the differences in the measurements of S_8 could well be due to modeling and other systematics [15].

The so-called lensing anomaly [2,16] is due to the fact that Planck CMB data shows a *preference* for additional lensing. CMB anisotropies get blurred due to gravitational lensing by the large scale structure of the Universe: Photons from different directions are mixed, and the peaks at large multipoles are smoothed. The amount of lensing is a precise prediction of the ΛCDM model: The consistency of the model can be checked by artificially increasing lensing by a factor $A_{\rm lens}$ [17] (*a priori* an unphysical parameter). If ΛCDM consistently describes all CMB data, observations should prefer $A_{\rm lens} = 1$. Intriguingly, Planck

[*]dengwang@ific.uv.es
[†]omena@ific.uv.es

CMB data shows a *preference* for additional lensing. Indeed, the reference analysis of temperature and polarization anisotropies suggest $A_{\rm lens} > 1$ at 3σ. CMB lensing also introduces a nontrivial four-point correlation function, and therefore, it can be independently measured. Adding this information somewhat diminishes the tension, albeit the value of the lensing amplitude is still above the canonical one by about 2σ. The lensing anomaly is robust against changes in the foreground modeling in the baseline likelihood and was already discussed in previous data releases, although it is currently more significant due to the lower reionization optical depth preferred by the Planck 2018 data release. Nevertheless, the deviation of $A_{\rm L}$ from its standard value could have its origin in other physics unrelated to lensing effects. Results from the Atacama Cosmology Telescope is compatible with $A_{\rm lens} = 1$ [18], but the results are consistent with Planck within uncertainties.

It is therefore extremely important to further test the ΛCDM paradigm at different epochs and scales. In this regard, future galaxy and weak lensing surveys will be able to test possible departures from the standard cosmological picture. Among the most appealing theoretical alternatives are those relying on modifications of general relativity at ultra large length scales. Usually, departures from general relativity are parametrized via the growth rate f [19–21]:

$$f \equiv \frac{d}{d\ln a}\frac{\delta(k,a)}{\delta(k,a_i)} = \Omega_m(a)^\gamma, \tag{1}$$

with

$$\Omega_m(a) = \Omega_{m0}a^{-3}/\left(\frac{H^2}{H_0^2}\right), \tag{2}$$

and, assuming a flat universe:

$$1 = \Omega_m(a) + \Omega_{\rm DE}(a). \tag{3}$$

Within the canonical general relativity scheme, and a flat ΛCDM background, $\gamma = 0.55$ [20,22]. Consequently, a departure from this standard value would suggest an inconsistency between the concordance cosmological model and observations. Recently, the authors of [26] have found a higher gravitational growth index than the canonical value $\gamma = 0.55$ when combining Planck CMB data with weak lensing, galaxy clustering and cosmic velocity observations. All in all, they find $\gamma = 0.633^{+0.025}_{-0.024}$, rejecting therefore with a significance of 3.7σ the standard value of γ. Previous studies [27,28] also find a similar value that is larger than 0.55 in light of the DES survey and different data combinations. The analysis of Ref. [26] makes use of a simple parametrization in terms of a unique parameter γ modifying the power spectrum as follows:

$$P(\gamma,k,a) = P(k,a=1)D^2(\gamma,a), \tag{4}$$

where the linear growth factor is related to the growth rate, Eq. (1), as

$$D(\gamma,a) = \exp-\left(\int_a^1 da\frac{\Omega_m(a)^\gamma}{a}\right). \tag{5}$$

Here we follow a different avenue and revise the current constraints on the growth of structure by means of an alternative parametrization and also considering CMB constraints both alone and in combination with other cosmological observations. Therefore, in order to include possible deviations from general relativity, instead of modifying the matter power spectrum via the growth factor f, we make use of a self-consistent parametrization in terms of two functions, $\mu(k,a)$ and $\eta(k,a)$, which modify the Poisson equation and introduce a gravitational slip, respectively [29]:

$$-k^2\Phi(k,a) \equiv 4\pi G a^2\mu(k,a)\rho(k,a)\delta(k,a); \tag{6}$$

$$\eta(k,a) \equiv \Psi(k,a)/\Phi(k,a), \tag{7}$$

where $\rho(a)$ is the average dark matter density, $\delta(k,a)$ is the comoving matter density contrast and Φ and Ψ are the gauge-invariant Bardeen potentials in the Newtonian gauge:

$$ds^2 = -(1+2\Phi)dt^2 + a^2(1-2\Psi)dx^2. \tag{8}$$

Using effective quantities like μ and η has the advantage that they are able to model any deviations of the perturbation behavior from ΛCDM expectations, they are relatively close to observations, and they can also be related to other commonly used parametrizations. Indeed, there is a direct relation between μ and γ [30], in such a way that it is always possible to map one parametrization $(\mu,\ \eta)$ into another related one $(\gamma,\ \eta)$:

$$\mu = \frac{2}{3}\Omega_m(a)^{\gamma-1}\left[\Omega_m(a)^\gamma + 2 - 3\gamma + \frac{3}{2}(\gamma-1)\Omega_m(a)\right], \tag{9}$$

for a flat ΛCDM universe and constant γ. In the following, we shall follow a parametrization in which the time evolution is related to the dark energy density fraction, i.e., a "late-time" parametrization [31], which also neglects the possible scale dependence of the functions μ and η:

$$\begin{aligned}\mu(a) &= 1 + E_{11}\Omega_{\rm DE}(a);\\ \eta(a) &= 1 + E_{22}\Omega_{\rm DE}(a).\end{aligned} \tag{10}$$

If $\mu_0 = \mu(a=1)$ and $\eta_0 = \eta(a=1)$, (E_{11}, E_{22}) is equivalent to (μ,η) at $a = 1$ today. We shall show our results for this parametrization. We also show results for the case in which we use (γ,η) as parameters describing the deviations with respect to the standard ΛCDM cosmology, by means

of Eqs. (9) and (10) as well as for the simplest one parameter γ case. The structure of the manuscript is as follows. Section II describes the numerical codes employed to develop our analyses and also the cosmological observations used along this study. Section III presents the constraints within the different growth of structure parametrizations from current data, the results from N-body simulations, and the future prospects for a Square Kilometer Array (SKA)-like survey. Finally, we draw our conclusions in Sec. IV.

II. METHODOLOGY

In order to study the constraints achievable by current CMB and large scale structure probes, we make use of the publicly available code MGCAMB [29,32–34], which is a modified version of CAMB [35] for cosmic structure growth, and incorporate the (γ, η) growth parametrization into it. We employ the Monte Carlo Markov Chain (MCMC) method to infer the posterior distributions of models parameters by using the code CosmoMC [36]. We analyze the MCMC chains via the public package GetDist [37]. Notice that we adopt the potential reduction scale factor $R-1=0.03$ proposed by Gelman and Rubin [38] as the convergence criterion of our MCMC analysis. We make use of the halofit numerical code [39–41] to model CMB lensing. We notice here that the use of this coded may introduce some uncertainties in the analyses, as it has not been properly modified to account for the growth extensions of our analyses. For all the growth parametrizations considered in this analysis, we choose the following uniform prior ranges for the different parameters: the baryon fraction $\Omega_b h^2 \in [0.005, 0.1]$, the cold dark matter fraction CDM fraction $\Omega_c h^2 \in [0.001, 0.99]$, the acoustic angular scale at recombination $100\theta_{\rm MC} \in [0.5, 10]$, the amplitude of primordial scalar power spectrum $\ln(10^{10}A_s) \in [2, 4]$, the scalar spectral index $n_s \in [0.8, 1.2]$, the reionization optical depth $\tau \in [0.01, 0.8]$, the CMB lensing amplitude $A_{\rm L} \in [0, 2.5]$, the amplitude of a lensing parameter, which is allowed to be an oscillatory function $A_\ell = A_{\rm L} + \sin \ell$, $A_{\rm M} \in [-1, 1]$, the growth index $\gamma \in [0, 1]$, the effective gravitational strength $\mu_0 \in [-3, 3]$ and the effective anisotropic stress $\eta_0 \in [-3, 3]$. In all the analyses presented in what follows, the parameters $\Omega_b h^2$, $\Omega_c h^2$, $100\theta_{\rm MC}$, $\ln(10^{10}A_s)$, n_s and τ are freely varying parameters.

Furthermore, to investigate the impacts of the growth index γ on cosmic structure formation, we modify the online software `Gadget2` [42]. Specifically, we modify the Poisson equation by replacing the factor $\mu(k, a)$ in Eq. (6) by Eq. (9), which characterizes the effective gravitational strength in this model. Note that we do not include the effect of anisotropic stress from photons and neutrino species on the large scale structure in this analysis. The background evolution of this model is equivalent to that of ΛCDM, since this model only considers the structure growth. As a consequence, we just need to consider the scalar density perturbation when making the initial condition. To simulate such a modified universe, at first, we use the best fit values of the model parameters from our conservative cosmological constraints as fiducial parameters. Then, using the code 2LPTic [43], we generate the initial condition at redshift $z = 49$ with 256^3 particles and a box size of $200h^{-1}$ Mpc and evolve the Universe to $z = 0$. The softening length we use is $15h^{-1}$ kpc in simulations. In order to study the effects of γ more clearly on structure formation, we also make a comparison group of simulations by only varying γ and fixing other parameters. We use the AHF code [44] to identify the dark halos and generate the halo catalogs in all the simulations.

Concerning the cosmological and astrophysical observations, our baseline datasets and likelihoods include:

(i) CMB. Observations from the Planck satellite have very important meanings for cosmology and astrophysics. They have measured the matter components, the topology and the large scale structure of the Universe. We therefore consider here Planck 2018 temperature and polarization (TT TE EE) data, and the low-ℓ temperature and polarization likelihoods at $\ell < 30$, namely TTTEEE + lowℓ + lowE [2,45–47]. We refer to this combination as "*C*."

(ii) Lensing. The CMB photons traverse almost the entire observable Universe to arrive here today and are deflected by gradients in the gravitational potentials associated with inhomogeneities in the Universe. We use the Planck 2018 lensing likelihood [48], reconstructed from measurements of the power spectrum of the lensing potential. We refer to this dataset as "*L*."

(iii) BAO. Baryon acoustic oscillations (BAO) are very clean observations to explore the evolution of the Universe, which are unaffected by uncertainties in the nonlinear evolution of the matter density field and by other systematic uncertainties that may affect other observations. Measuring the positions of these oscillations in the matter power spectrum at different redshifts can place strong constraints on the cosmic expansion history. We employ BAO measurements extracted from the 6dFGS [49], SDSS MGS [50], BOSS DR12 [51] and eBOSS DR16 [52,53] samples. We refer to this dataset combination as "*B*."

(iv) SNIa. Supernovae Ia luminosity distances are powerful distance indicators to probe the expansion history of the Universe, especially, the equation of state of the dark energy component. We adopt SNIa data points from the largest Pantheon + sample [54], which is made of 1701 light curves of 1550 spectroscopically confirmed SNe Ia coming from 18 different surveys. This updated sample has a significant improvement relative to Pantheon [55], especially at low redshifts, and covers the redshift range $z \in [0.000122, 2.26137]$. We refer to this dataset combination as "*S*."

In what follows, we shall report results for CMB alone ("*C*"), CMB plus CMB lensing ("CL"), CMB plus BAO plus supernovae Ia datasets ("CBS") and CMB plus BAO plus supernovae Ia plus CMB lensing ("CBSL").

Notice that we do not consider weak lensing data in our baseline data analysis. Despite these measurements having been considered in previous works [26], in order to properly compute the weak lensing observables, one would need to modify accordingly to the parametrization used here [see Eqs. (9) and (10)] the halofit [39–41] numerical code. In the absence of a publicly available modified version of the former code, we follow here a very conservative approach, neglecting the weak lensing input in our baseline data analysis.

The most conservative data combination is therefore what we refer to *CBS*, i.e., CMB, BAO and SNIa observations. Such a data combination will be enlarged with weak lensing and RSD measurements for the sake of comparison with previous studies [26].

To investigate the observational viability of different growth parametrizations, taking ΛCDM as the reference model, we compute the Bayesian evidences of nine models, ε_i, and Bayes factor, $B_{ij} = \varepsilon_i/\varepsilon_j$, where ε_j is the statistical evidence of the reference model. According to Ref. [56], we employ a revised and more conservative version of the so-called Jeffreys' scale; i.e., $\ln B_{ij} = 0$–1, $\ln B_{ij} = 1$–2.5, $\ln B_{ij} = 2.5$–5 and $\ln B_{ij} > 5$ indicate an *inconclusive*, *weak*, *moderate* and *strong* preference of the model i relative to the reference model j. It is noteworthy that if $\ln B_{ij} < 0$ for an experiment, it implies that data prefers the reference model.

TABLE I. Bayesian factor for different models in light of Planck-2018 CMB data.

Models	$\ln B_{ij}$
ΛCDM	0
ΛCDM + $A_{\rm L}$	−1.154
ΛCDM + $A_\ell + A_m$	−2.511
γ	−0.997
$\gamma + A_{\rm L}$	−3.104
γ, η	−0.053
$\gamma, \eta + A_{\rm L}$	−2.133
μ, η	1.397
$\mu, \eta + A_{\rm L}$	−0.501
$\mu, \eta + A_\ell + A_m$	−2.444

III. RESULTS

A. Constraints from CMB, large scale structure and supernovae Ia data

Table I summarizes our results concerning the Bayesian preference for different models versus the canonical ΛCDM scenario arising from CMB observations, including also CMB lensing in our analyses. Notice that a model with both (μ, η) as free parameters is substantially preferred over the canonical ΛCDM scenario. We show the time dependence of μ [that is, $\mu(a)$; see Eq. (10)] in the left panel of Fig. 1 from CMB plus CMB lensing measurements. The right panel depicts the equivalence between the γ parameter and the $\mu(z)$ one: an enhancement of the growth of structure today, characterized by $\gamma < 0.55$, implies $\mu(z) > 1$ and $\mu_0 - 1 > 0$. As it is clear from the left panel of Fig. 1, since a value of $\mu > 1$ is reconstructed from CMB temperature, polarization and lensing data, this would imply an enhancement of the growth of structure. Concerning the parametrization in terms of (μ, η), it is almost equally favored as the ΛCDM cosmology. Notice however that the parametrization that only makes use of the γ parameter is disfavored. The left panels of Figs. 2 and 3 depict the 68% and 95% CL allowed contours from Planck CMB data, with and without CMB lensing, in the $(\mu_0 - 1, \eta_0 - 1)$ and $(\gamma, \eta_0 - 1)$ planes, associated to the (μ, η) and (γ, η) parametrizations, respectively.

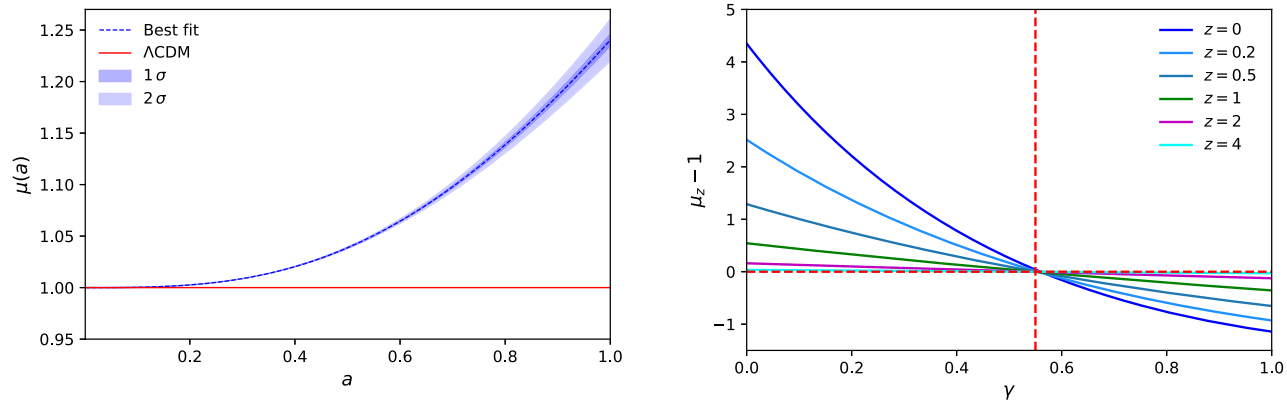

FIG. 1. Left panel: time dependence of the parameter $\mu(a)$ together with the 1 and 2σ errors from CMB temperature and polarization plus CMB lensing measurements. Right panel: equivalence between the γ parameter and $\mu(z) - 1$; see Eq. (9), for a number of different redshifts. The cross point corresponds to ΛCDM and the horizontal and vertical dashed lines depict the expectations within standard cosmology, i.e., $\mu = 1$ and $\gamma = 0.55$ respectively.

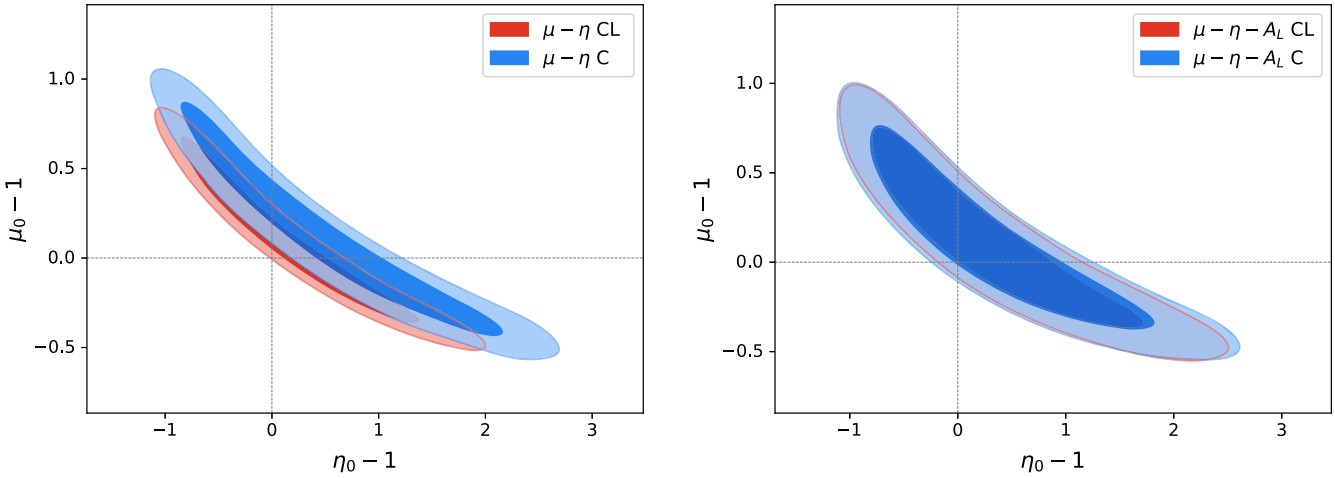

FIG. 2. Left panel: 68% and 95% CL contours in the $(\eta_0 - 1, \mu_0 - 1)$ plane within the growth model parametrized via μ and η, see Eq. (10), obtained by using CMB temperature and polarization measurements (blue contours) and CMB temperature, polarization and lensing observations (red contours). Right panel: as in the left panel but when the lensing amplitude $A_{\rm L}$ is also considered as a freely varying parameter.

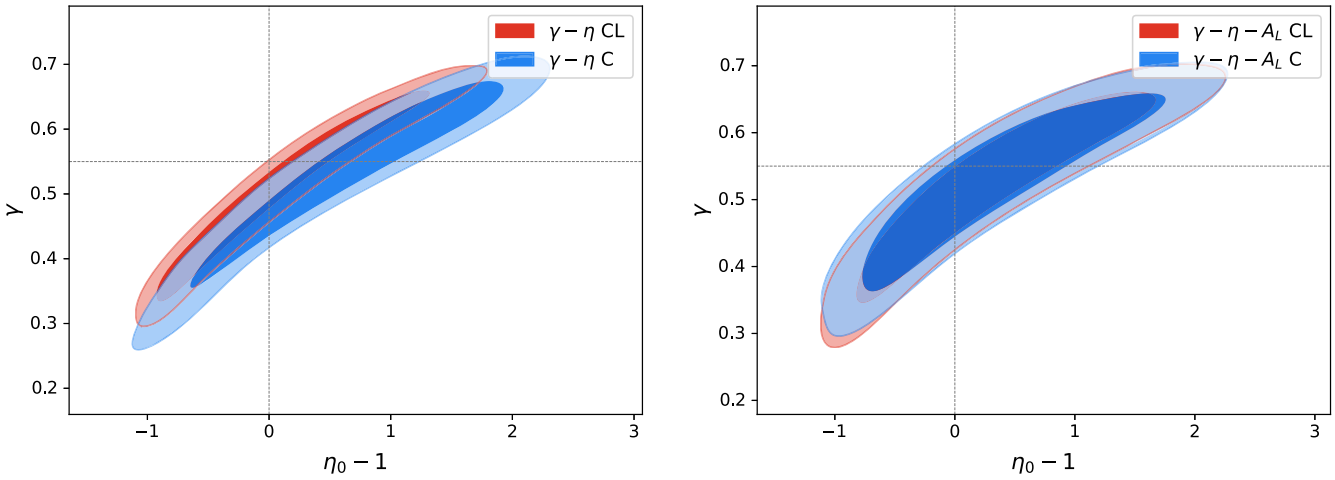

FIG. 3. Left panel: 68% and 95% CL contours in the $(\eta_0 - 1, \gamma)$ plane within the growth model parametrized via γ and η; see Eq. (9) and the second of Eq. (10) obtained by using CMB temperature and polarization measurements (blue contours) and CMB temperature, polarization and lensing observations (red contours). Right panel: as in the left panel but when the lensing amplitude $A_{\rm L}$ is also considered as a freely varying parameter.

We start reporting the values of the most relevant parameters in what follows. Table II depicts the results for the simplest growth parametrization in terms of a single parameter γ, for the sake of comparison with previous results [26]. Notice that, contrary to the results previously quoted in the literature, we obtain always $\gamma < 0.55$, i.e., *an enhanced growth of structure today*, in agreement also with the results depicted in Figs. 2 and 3. Notice that CMB alone prefers $\gamma < 0.55$ ($\gamma = 0.506 \pm 0.022$) at 3σ level. The addition of SNIa and BAO measurements do not change this preference, while the addition of CMB lensing relaxes the preference to the 2σ level ($\gamma = 0.468^{+0.017}_{-0.029}$). This is related to the fact that the lensing data restores the value of the lensing amplitude to its standard expectation of $A_{\rm L} = 1$ when this parameter is freely varying. However, in this case, this parameter is fixed, and therefore, a reduced growth of structure can mimic the very same effect. Consequently, the value of the growth index γ approaches the standard one when including CMB lensing in the data analyses, i.e., shifts to larger values, getting closer to $\gamma = 0.55$. As can be noticed from Table II, the values of the Hubble parameter are not significantly shifted, and therefore, this simplest model does not ameliorate the so-called H_0 tension.

The values of the S_8 parameter are instead lower than within the minimal ΛCDM cosmology and closer to those

TABLE II. Mean values and 68% CL marginalized errors of the most relevant cosmological parameters within the growth model parametrized via γ, obtained by using the CMB plus lensing, CMB alone, CMB plus BAO plus supernovae Ia plus lensing and CMB plus BAO plus supernovae Ia datasets, respectively.

Parameters	CL	C	CBSL	CBS
$\Omega_b h^2$	0.02228 ± 0.00016	0.02253 ± 0.00016	0.02246 ± 0.00013	0.02250 ± 0.00014
$\Omega_c h^2$	0.1186 ± 0.0014	0.1186 ± 0.0015	0.11901 ± 0.00096	0.11910 ± 0.00099
$100\theta_{MC}$	1.04107 ± 0.00032	1.04109 ± 0.00033	1.04100 ± 0.00029	1.04102 ± 0.00030
τ	$0.0495^{+0.0083}_{-0.0075}$	0.0517 ± 0.0077	$0.0494^{+0.0082}_{-0.0074}$	0.0511 ± 0.0077
$\ln(10^{10}A_s)$	$3.030^{+0.018}_{-0.015}$	3.036 ± 0.016	3.031 ± 0.017	3.036 ± 0.016
n_s	0.9684 ± 0.0046	0.9689 ± 0.0047	0.9671 ± 0.0037	0.9677 ± 0.0039
γ	0.506 ± 0.022	$0.468^{+0.017}_{-0.029}$	$0.511^{+0.022}_{-0.019}$	$0.470^{+0.017}_{-0.029}$
H_0	68.02 ± 0.64	68.03 ± 0.67	67.80 ± 0.43	67.82 ± 0.44
Ω_m	0.3064 ± 0.0085	0.3066 ± 0.0089	0.3092 ± 0.0057	0.3093 ± 0.0059
σ_8	0.8149 ± 0.0062	$0.8299^{+0.0092}_{-0.0080}$	0.8149 ± 0.0063	$0.8302^{+0.0093}_{-0.0082}$
S_8	0.823 ± 0.013	0.839 ± 0.016	0.827 ± 0.010	0.843 ± 0.012
χ^2	2785.6	2772.6	3841.4	3828.7

obtained from weak lensing probes, alleviating therefore the so-called S_8 tension. Indeed, the mean values of S_8 are very similar to those reported when combining CMB data with observations from the Dark Energy Survey (DES). The difference within this simplest model in the values of γ obtained here and those reported in Ref. [26] can be due to a number of differences among the two analyses. Namely, here we modify the evolution of the two gravitational potentials rather than simply changing the matter power spectrum evolution. Also, we do not make use of datasets that may require the use of the halofit numerical code, which has not been properly modified to account for departures from the canonical growth of structure. As previously argued, this is the main reason to not to exploit weak lensing observations in almost all the results shown here. Figure 4 shows the fact that, if we include the very same observations as those considered in Ref. [26], we get the opposite to what we report here, i.e., a reduced growth factor characterized by $\mu_0 - 1 < 0$, or, equivalently, by $\gamma > 0.55$. The additional datasets considered in Fig. 4 are the Dark Energy Survey 1 large scale structure observations,[1] which includes the following three two-point correlation functions: (i) galaxy clustering. In general, the homogeneity of matter distribution in the Universe can be traced by galaxies distribution. The overabundance of pairs at angular separation θ in a random distribution, $\omega(\theta)$, is one of the most convenient ways to measure galaxy clustering. It quantifies the scale dependence and strength of galaxy clustering and consequently affects the matter clustering. (ii) Cosmic shear. The two-point statistics characterize shapes of galaxies are very complex, since they are products of components of a spin-2 tensor. Therefore, it is convenient to extract information from a galaxy survey by using a pair of two-point correlation functions $\xi_+(\theta)$ and $\xi_-(\theta)$, which denote the sum and difference of products of tangential and cross components of the shear, measured with respect to the line connecting each pair of galaxies. (iii) Galaxy-galaxy lensing. The characteristic distortion of source galaxy shapes is from masses associated with foreground lenses. This distortion is the mean tangential ellipticity of source galaxy shapes around lens galaxy positions for each pair of redshift bins and also named as the tangential shear, $\zeta_t(\theta)$. This dataset is referred to as DESY1 [57–61]. We also include the measurements of $f\sigma_8$, with being σ_8 the clustering parameter, extracted from both peculiar velocity and redshift-space distortion (RSD) data [52,62–71]. Specifically, we use the so-called "Gold-2017" growth-rate dataset [72]. We refer this dataset as "RSD."

Table III shows the mean values and the errors obtained via the parametrization given by Eq. (10). Notice that for all the data combinations, there are not significant departures from the standard cosmological expectations $\mu_0 = \eta_0 = 1$, but, if any, *they always imply a larger growth, i.e.,* $\gamma < 0.55$, and not a reduced one, as claimed by Ref. [26] due to a partial parametrization of the growth effects, only included in the matter power spectrum. The situation with the H_0 and S_8 tensions is very similar to that observed within the γ-only parametrization. Nevertheless, the value of the parameter S_8 is further reduced in this case, improving therefore the consistency on the values of this parameter obtained by CMB observations and by weak lensing probes. Table IV shows the mean values and the errors obtained via the parametrization given by Eq. (9) and the second of Eq. (10). Notice that from CMB data alone, there is a 2σ preference for $\gamma < 0.55$. In this case, when we add lensing observations, the significance is improved to the 3σ level, but the mean value of η_0 gets closer to 1. Therefore, as long as CMB lensing observations are considered, there is a 3σ preference for a

[1] https://github.com/cmbant/CosmoMC/tree/master/data/DES.

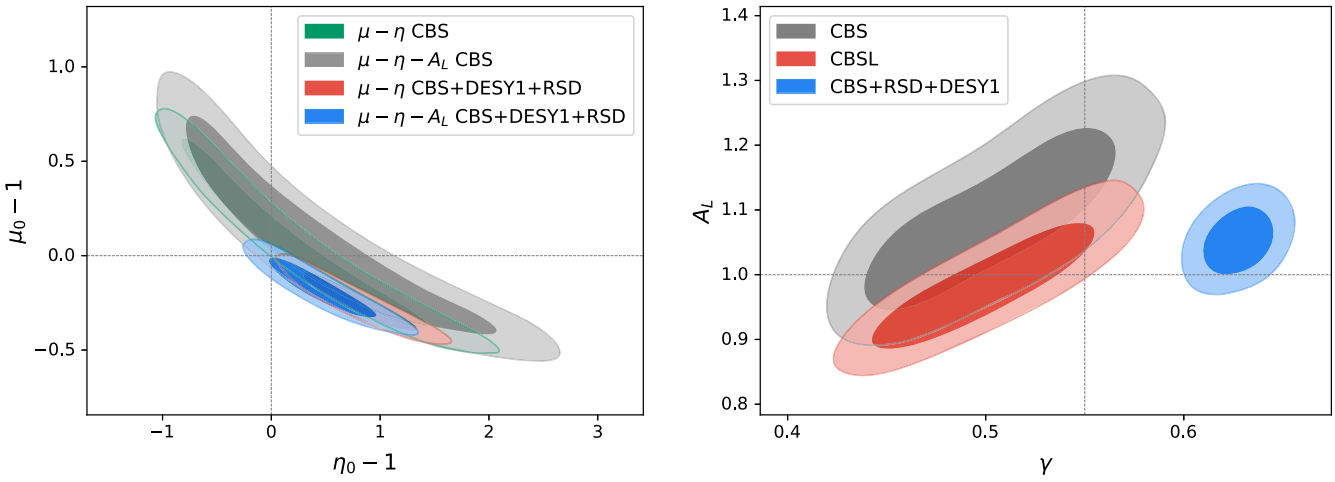

FIG. 4. Left panel: the red regions depict the 68% and 95% CL contours in the $(\eta_0 - 1, \mu_0 - 1)$ plane within the growth model parametrized via μ and η; see Eq. (10) obtained by using CMB temperature and polarization measurements, BAO, SNIa, weak lensing and RSD measurements. The blue regions depict the equivalent but when the lensing amplitude $A_{\rm L}$ is also considered as a freely varying parameter. Right panel: allowed regions in the simplest growth parametrization used here, i.e., via just one single parameter γ in the (γ, $A_{\rm L}$) plane allowed from different datasets, for the sake of comparison with the results of Ref. [26]. Thee horizontal and vertical lines depict the expectations within the canonical ΛCDM cosmology, i.e., $A_{\rm L} = 1$ and $\gamma = 0.55$, respectively.

growth enhancement, while if these observations are not considered, such a preference is reduced to the 2σ level.

B. CMB lensing amplitude $A_{\rm L}$

The values of γ and η reported above clearly show that there is a preference for an enhanced growth of structure from CMB observations, either alone or combined with BAO and SNIa luminosity distances. The larger growth that we obtain at late times would increase CMB lensing, probably suggesting a degeneracy with the lensing amplitude $A_{\rm L} > 1$. Consequently, we perform also here analysis in which this parameter is a freely varying one. Table I shows that the extension of the ΛCDM model with $A_{\rm L}$ is moderately disfavored with respect to the minimal scenario. More importantly here, the (γ, η) plus $A_{\rm L}$ case is weakly disfavored since, as we have already discussed, the γ parameter and the lensing amplitude have the very same effect in the lensing observables due to large scale structure effects.

Based on the fact that full CMB data prefers a anomalous lensing amplitude $A_{\rm L} > 1$, we aim at exploring phenomenologically the possible origin of this lensing anomaly. One possibility is that $A_{\rm L}$ may have an angular scale dependence. Specifically, we assume A_ℓ as an oscillatory function of the multipole ℓ; i.e., $A_\ell = A_{\rm L} + A_m \sin \ell$. This

TABLE III. Mean values and 68% CL marginalized errors of the most relevant cosmological parameters within the growth model parametrized via μ and η, see Eq. (10), obtained by using the CMB plus lensing, CMB alone, CMB plus BAO plus supernovae Ia plus lensing and CMB plus BAO plus supernovae Ia datasets, respectively.

Parameters	CL	C	CBSL	CBS
$\Omega_b h^2$	0.02251 ± 0.00016	0.02257 ± 0.00017	0.02247 ± 0.00013	0.02254 ± 0.00014
$\Omega_c h^2$	0.1184 ± 0.0014	0.1182 ± 0.0015	0.11885 ± 0.00094	0.1188 ± 0.0010
$100\theta_{MC}$	1.04109 ± 0.00032	1.04112 ± 0.00033	1.04102 ± 0.00029	$1.04103^{+0.00026}_{-0.00031}$
τ	$0.0491^{+0.0082}_{-0.0074}$	0.0508 ± 0.0082	$0.0484^{+0.0083}_{-0.0073}$	$0.0497^{+0.0084}_{-0.0071}$
$\ln(10^{10} A_s)$	3.029 ± 0.017	3.033 ± 0.017	$3.028^{+0.017}_{-0.015}$	$3.033^{+0.018}_{-0.015}$
n_s	0.9691 ± 0.0045	0.9701 ± 0.0050	0.9679 ± 0.0037	0.9684 ± 0.0039
$\mu_0 - 1$	$0.09^{+0.28}_{-0.40}$	$0.13^{+0.28}_{-0.52}$	$0.06^{+0.27}_{-0.38}$	$0.08^{+0.27}_{-0.47}$
$\eta_0 - 1$	$0.23^{+0.57}_{-0.91}$	$0.56^{+0.70}_{-1.30}$	$0.26^{+0.57}_{-0.92}$	$0.62^{+0.84}_{-1.10}$
H_0	68.11 ± 0.64	68.21 ± 0.71	67.88 ± 0.42	67.89 ± 0.45
Ω_m	0.3052 ± 0.0084	0.3042 ± 0.0094	0.3082 ± 0.0056	0.3084 ± 0.0060
σ_8	$0.810^{+0.032}_{-0.038}$	$0.815^{+0.031}_{-0.053}$	$0.808^{+0.030}_{-0.038}$	$0.813^{+0.029}_{-0.049}$
S_8	0.817 ± 0.035	$0.821^{+0.039}_{-0.051}$	0.819 ± 0.034	$0.824^{+0.033}_{-0.050}$
χ^2	2785.8	2772.8	3841.8	3828.6

TABLE IV. Mean values and 68% CL marginalized errors of the most relevant cosmological parameters within the growth model parametrized via γ and η, see Eq. (9) and the second of Eq. (10), obtained by using the CMB plus lensing, CMB alone, CMB plus BAO plus supernovae Ia plus lensing and CMB plus BAO plus supernovae Ia datasets, respectively.

Parameters	CL	C	CBSL	CBS
$\Omega_b h^2$	0.02250 ± 0.00016	0.02256 ± 0.00017	0.02246 ± 0.00014	0.02252 ± 0.00014
$\Omega_c h^2$	0.1185 ± 0.0014	0.1183 ± 0.0015	0.11901 ± 0.00098	0.1190 ± 0.0010
$100\theta_{MC}$	1.04107 ± 0.00032	1.04111 ± 0.00033	1.04101 ± 0.00029	1.04106 ± 0.00029
τ	0.0489 ± 0.0084	0.0501 ± 0.0083	$0.0486^{+0.0082}_{-0.0073}$	0.0505 ± 0.0079
$\ln(10^{10}A_s)$	3.029 ± 0.017	3.032 ± 0.018	3.029 ± 0.017	3.034 ± 0.017
n_s	0.9687 ± 0.0046	0.9696 ± 0.0051	0.9674 ± 0.0038	0.9683 ± 0.0038
γ	$0.513^{+0.130}_{-0.088}$	$0.532^{+0.130}_{-0.065}$	$0.513^{+0.120}_{-0.086}$	$0.529^{+0.130}_{-0.071}$
η_0-1	$0.14^{+0.47}_{-1.00}$	$0.64^{+0.97}_{-0.75}$	$0.10^{+0.46}_{-0.94}$	$0.57^{+0.88}_{-0.79}$
H_0	68.06 ± 0.65	68.17 ± 0.70	67.81 ± 0.44	67.88 ± 0.45
Ω_m	0.3058 ± 0.0086	0.3047 ± 0.0093	0.3091 ± 0.0059	0.3085 ± 0.0060
σ_8	$0.813^{+0.030}_{-0.040}$	$0.808^{+0.021}_{-0.042}$	$0.815^{+0.028}_{-0.038}$	$0.812^{+0.022}_{-0.042}$
S_8	0.821 ± 0.037	$0.815^{+0.029}_{-0.047}$	$0.827^{+0.032}_{-0.038}$	$0.823^{+0.026}_{-0.044}$
χ^2	2786.0	2772.9	3841.9	3828.6

model is a weakly or moderately disfavored scenario, either within the minimal ΛCDM cosmology or within the (μ, η) parametrization.

The right panels of Figs. 2 and 3 depict the 68% and 95% CL allowed contours from Planck CMB data, with and without CMB lensing, in the $(\mu_0 - 1, \eta_0 - 1)$ and $(\gamma, \eta_0 - 1)$ planes, associated to the (μ, η) and (γ, η) parametrizations respectively, with $A_{\rm L}$ a freely varying parameter in the data analyses. Notice that the mean values of γ are now shifted toward its expectation within the ΛCDM cosmology, $\gamma = 0.55$. Figure 4 (left panel) shows that the reduced growth of structure favored by weak lensing, and RSD observations is less evident when adding $A_{\rm L}$ as a free parameter. The presence of a varying lensing amplitude restores the canonical values for $(\mu_0 - 1, \eta_0 - 1)$, i.e., shifts their values toward (0,0). It is easy to see that the inclusion of weak lensing and RSD data can significantly improve the constraining power on modified growth. The right panel of Fig. 4 clearly illustrates the large degeneracy between $A_{\rm L}$ and γ within the simplest growth model explored here, i.e., the one with one single parameter γ. Notice that the effect of a larger lensing amplitude $A_{\rm L}$ can be compensated with a smaller growth of structure, i.e., a value of γ closer to the standard expectation of $\gamma = 0.55$ in the case of the CBS and CBSL datasets. When considering also RSD and DESY1 measurements, the mean value of $\gamma > 0.55$ but the very same degeneracy holds; i.e., larger lensing amplitudes are correlated with a smaller growth of structure ($\gamma > 0.55$).

The fact that both γ and $A_{\rm L}$ have a very similar impact in the CMB lensing power spectra at late times is also explicitly shown in Fig. 5. The left panel shows the CMB lensed power spectrum, together with Planck 2018 observations [48] for several possible scenarios. In the case of ΛCDM plus $A_{\rm L}$, we have fixed the former parameter to 1.07, which is the best fit from Planck temperature, polarization and lensing data. Notice that, if $\gamma < 0.55$,

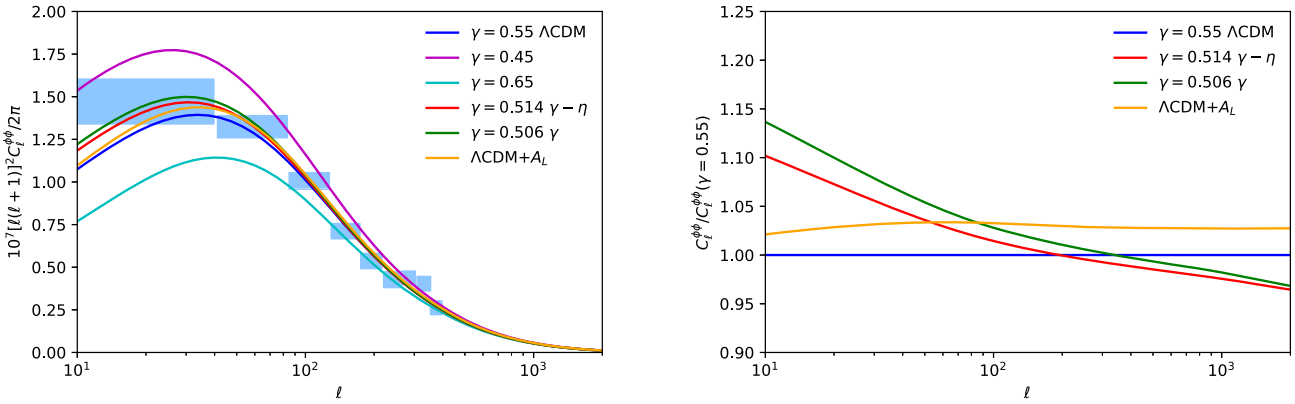

FIG. 5. Left panel: CMB lensed power spectrum, together with Planck 2018 measurements for several possible scenarios; see text for details. Right panel: deviation of the lensing potential with respect to the ΛCDM case for different growth parametrizations.

the lensing power spectrum is enhanced, due to a larger growth of structure. The very same enhancement is obtained by a value of $A_{\rm L} > 1$. The right panel of Fig. 5 depicts the deviation of the lensing potential with respect to the ΛCDM case for the different growth parametrizations exploited here. Notice that for multipoles $\ell < 200$, the lensing power spectrum is larger than that expected within the canonical scenario if either $\gamma < 0.55$ or $A_{\rm L} > 1$.

Table V shows the preferred values for the lensing amplitude $A_{\rm L}$ within the minimal ΛCDM universe from the different data combinations considered here. While CMB data (either alone or in combination with BAO and SNIa measurements) prefers $A_{\rm L} > 1$ with $\sim 3\sigma$ significance, the addition of CMB lensing observations softens this preference to the 2σ level.

Table VI depicts the equivalent to Table II but leaves $A_{\rm L}$ as a free parameter. Notice that we obtain values of $\gamma < 0.55$ always, but the statistical significance for such a preference is decreased due to the fact that γ is degenerate with the lensing amplitude; i.e., a lower value of γ can be compensated with a lower value of $A_{\rm L}$ and also because lensing observations prefer a lower value of the lensing amplitude. The preference for $\gamma < 0.55$ decreases to the $1-2\sigma$ significance level, depending on the datasets. Furthermore, when CMB lensing observations are considered, the mean value of $A_{\rm L} < 1$.

Table VII shows the equivalent to Table III but when $A_{\rm L}$ is a free parameter; i.e., the mean values and the errors obtained via the parametrization given by Eq. (10) plus a freely varying lensing amplitude parameter. As in the

TABLE V. Mean values and 68% CL marginalized errors of the most relevant cosmological parameters within the ΛCDM cosmology when the lensing amplitude is also a freely varying parameter. We report the results obtained by using the CMB plus lensing, CMB alone, CMB plus BAO plus supernovae Ia plus lensing and CMB plus BAO plus supernovae Ia datasets, respectively.

Parameters	CL	C	CBSL	CBS
$\Omega_b h^2$	0.02251 ± 0.00017	0.02259 ± 0.00017	0.02247 ± 0.00014	0.02254 ± 0.00014
$\Omega_c h^2$	0.1182 ± 0.0015	0.1181 ± 0.0016	0.11894 ± 0.00098	0.11887 ± 0.00095
$100\theta_{MC}$	1.04110 ± 0.00032	1.04114 ± 0.00032	1.04102 ± 0.00029	1.04105 ± 0.00029
τ	$0.0491^{+0.0086}_{-0.0076}$	$0.0492^{+0.0088}_{-0.0073}$	$0.0493^{+0.0087}_{-0.0073}$	0.0501 ± 0.0086
$\ln(10^{10}A_s)$	$3.029^{+0.018}_{-0.016}$	$3.029^{+0.018}_{-0.015}$	$3.030^{+0.018}_{-0.015}$	3.033 ± 0.018
n_s	0.9696 ± 0.0048	$0.9708 \pm y0.0048$	0.9679 ± 0.0038	0.9688 ± 0.0037
$A_{\rm L}$	$1.071^{+0.038}_{-0.042}$	1.180 ± 0.065	$1.060^{+0.032}_{-0.037}$	$1.158^{+0.056}_{-0.063}$
H_0	68.16 ± 0.70	68.28 ± 0.72	67.85 ± 0.46	67.94 ± 0.45
Ω_m	0.3045 ± 0.0092	0.3033 ± 0.0094	0.3087 ± 0.0060	0.3078 ± 0.0058
σ_8	0.7999 ± 0.0086	0.7997 ± 0.0090	0.8026 ± 0.0078	0.8034 ± 0.0077
S_8	0.806 ± 0.019	0.804 ± 0.019	0.814 ± 0.013	0.814 ± 0.013
χ^2	2786.9	2773.0	3843.0	3829.4

TABLE VI. Mean values and 68% CL marginalized errors of the most relevant cosmological parameters within the growth model parametrized via one single parameter γ, when the lensing amplitude is also a freely varying parameter. We report the results obtained by using the CMB plus lensing, CMB alone, CMB plus BAO plus supernovae Ia plus lensing and CMB plus BAO plus supernovae Ia datasets, respectively.

Parameters	CL	C	CBSL	CBS
$\Omega_b h^2$	0.02249 ± 0.00017	0.02258 ± 0.00017	$0.02246^{+0.00013}_{-0.00015}$	0.02254 ± 0.00014
$\Omega_c h^2$	0.1185 ± 0.0015	0.1182 ± 0.0016	0.11907 ± 0.00097	0.1188 ± 0.0010
$100\theta_{MC}$	1.04106 ± 0.00032	1.04114 ± 0.00033	1.04100 ± 0.00030	1.04104 ± 0.00031
τ	$0.0506^{+0.0078}_{-0.0071}$	$0.0525^{+0.0088}_{-0.0067}$	$0.0495^{+0.0088}_{-0.0077}$	$0.0490^{+0.0083}_{-0.0074}$
$\ln(10^{10}A_s)$	3.032 ± 0.017	$3.037^{+0.019}_{-0.014}$	$3.032^{+0.018}_{-0.016}$	$3.031^{+0.018}_{-0.016}$
n_s	0.9687 ± 0.0048	0.9701 ± 0.0050	0.9672 ± 0.0039	0.9685 ± 0.0038
$A_{\rm L}$	$0.991^{+0.057}_{-0.075}$	$1.085^{+0.075}_{-0.098}$	$0.984^{+0.056}_{-0.071}$	$1.086^{+0.080}_{-0.097}$
γ	0.501 ± 0.036	$0.497^{+0.036}_{-0.045}$	$0.511^{+0.022}_{-0.019}$	$0.503^{+0.041}_{-0.047}$
H_0	68.03 ± 0.69	68.23 ± 0.72	67.79 ± 0.45	67.94 ± 0.47
Ω_m	0.3062 ± 0.0092	0.3041 ± 0.0095	0.3095 ± 0.0059	0.3077 ± 0.0061
σ_8	$0.817^{+0.016}_{-0.014}$	$0.820^{+0.017}_{-0.013}$	$0.819^{+0.015}_{-0.013}$	0.817 ± 0.015
S_8	0.826 ± 0.022	$0.825^{+0.024}_{-0.022}$	0.832 ± 0.018	0.827 ± 0.019
χ^2	2786.1	2772.9	3842.3	3829.1

TABLE VII. Mean values and 68% CL marginalized errors of the most relevant cosmological parameters within the growth model parametrized via μ and η, see Eq. (10), when the lensing amplitude is also a freely varying parameter. We report the results obtained by using the CMB plus lensing, CMB alone, CMB plus BAO plus supernovae Ia plus lensing and CMB plus BAO plus supernovae Ia datasets, respectively.

Parameters	CL	C	CBSL	CBS
$\Omega_b h^2$	0.02249 ± 0.00017	0.02259 ± 0.00017	0.02246 ± 0.00014	0.02252 ± 0.00014
$\Omega_c h^2$	0.1186 ± 0.0015	0.1181 ± 0.0015	0.1190 ± 0.0010	0.11884 ± 0.00099
$100\theta_{MC}$	1.04107 ± 0.00033	1.04115 ± 0.00032	1.04100 ± 0.00029	1.04104 ± 0.00030
τ	$0.0496^{+0.0084}_{-0.0073}$	$0.0498^{+0.0085}_{-0.0075}$	0.0493 ± 0.0085	0.0494 ± 0.0082
$\ln(10^{10}A_s)$	$3.030^{+0.018}_{-0.015}$	3.030 ± 0.017	$3.031^{+0.018}_{-0.016}$	3.032 ± 0.018
n_s	0.9685 ± 0.0049	0.9706 ± 0.0048	0.9675 ± 0.0039	0.9688 ± 0.0039
$A_{\rm L}$	$0.958^{+0.062}_{-0.080}$	$1.062^{+0.082}_{-0.110}$	$0.08^{+0.25}_{-0.48}$	$1.041^{+0.082}_{-0.100}$
μ_0-1	$0.12^{+0.29}_{-0.44}$	$0.11^{+0.28}_{-0.46}$	$0.06^{+0.27}_{-0.38}$	$0.12^{+0.29}_{-0.46}$
η_0-1	$0.35^{+0.54}_{-1.10}$	$0.39^{+0.59}_{-1.10}$	$0.47^{+0.60}_{-1.20}$	$0.40^{+0.59}_{-1.20}$
H_0	68.00 ± 0.69	68.29 ± 0.71	67.80 ± 0.46	67.94 ± 0.46
Ω_m	0.3066 ± 0.0092	0.3031 ± 0.0093	0.3092 ± 0.0061	0.3078 ± 0.0060
σ_8	$0.814^{+0.032}_{-0.045}$	$0.812^{+0.031}_{-0.046}$	$0.812^{+0.028}_{-0.047}$	$0.815^{+0.031}_{-0.047}$
S_8	$0.823^{+0.038}_{-0.046}$	$0.816^{+0.037}_{-0.046}$	$0.824^{+0.032}_{-0.048}$	$0.826^{+0.034}_{-0.047}$
χ^2	2786.5	2773.1	3842.4	3829.4

TABLE VIII. Mean values and 68% CL marginalized errors of the most relevant cosmological parameters within the growth model parametrized via γ and η, see Eq. (9) and the second of Eq. (10), when the lensing amplitude is also a freely varying parameter. We report the results obtained by using the CMB plus lensing, CMB alone, CMB plus BAO plus supernovae Ia plus lensing and CMB plus BAO plus supernovae Ia datasets, respectively.

Parameters	CL	C	CBSL	CBS
$\Omega_b h^2$	0.02248 ± 0.00016	0.02260 ± 0.00017	0.02245 ± 0.00014	0.02254 ± 0.00014
$\Omega_c h^2$	0.1186 ± 0.0015	0.1180 ± 0.0016	0.1191 ± 0.0010	0.1189 ± 0.0010
$100\theta_{MC}$	1.04107 ± 0.00032	1.04115 ± 0.00033	1.04101 ± 0.00029	1.04104 ± 0.00029
τ	$0.0492^{+0.0086}_{-0.0074}$	$0.0494^{+0.0086}_{-0.0077}$	$0.0492^{+0.0083}_{-0.0074}$	0.0500 ± 0.0078
$\ln(10^{10}A_s)$	$3.029^{+0.018}_{-0.016}$	$3.030^{+0.018}_{-0.016}$	3.031 ± 0.017	3.033 ± 0.017
n_s	0.9684 ± 0.0047	0.9706 ± 0.0049	0.9674 ± 0.0038	0.9687 ± 0.0039
$A_{\rm L}$	$0.971^{+0.063}_{-0.078}$	$1.078^{+0.080}_{-0.110}$	$0.962^{+0.060}_{-0.073}$	$1.059^{+0.080}_{-0.093}$
γ	$0.527^{+0.130}_{-0.071}$	$0.528^{+0.120}_{-0.076}$	$0.523^{+0.130}_{-0.075}$	$0.526^{+0.110}_{-0.077}$
η_0-1	$0.36^{+0.65}_{-1.00}$	$0.36^{+0.63}_{-1.00}$	$0.35^{+0.60}_{-1.10}$	$0.36^{+0.71}_{-0.91}$
H_0	67.99 ± 0.68	68.32 ± 0.72	67.79 ± 0.45	67.94 ± 0.45
Ω_m	0.3067 ± 0.0091	0.3029 ± 0.0094	0.3095 ± 0.0060	0.3078 ± 0.0060
σ_8	$0.810^{+0.024}_{-0.041}$	$0.808^{+0.024}_{-0.038}$	$0.813^{+0.023}_{-0.041}$	$0.812^{+0.024}_{-0.038}$
S_8	$0.819^{+0.032}_{-0.044}$	$0.811^{+0.031}_{-0.041}$	$0.825^{+0.027}_{-0.042}$	$0.822^{+0.027}_{-0.040}$
χ^2	2786.5	2773.1	3842.1	3829.2

$A_{\rm L} = 1$ case, for all the data combinations explored here, there are not significant departures from the standard cosmological expectations $\mu_0 = \eta_0 = 1$, but, if any, *they always imply a larger growth, i.e.,* $\gamma < 0.55$, and not a reduced one. As in the previous case, we no longer observe a significant preference for $A_{\rm L} > 1$, being this parameter smaller than 1 when CMB lensing observations are included in the data analyses. This is related to the degeneracy between $A_{\rm L}$ and the (μ, η) parametrization and also to the fact that CMB lensing measurements prefer a lensing amplitude closer to the standard value $A_{\rm L} = 1$.

Table VIII shows the equivalent to Table IV but leaves $A_{\rm L}$ as a free parameter, that is, presents the results in the parametrization given by Eq. (9) and the second of Eq. (10). In this case, there is always a 2σ preference for $\gamma < 0.55$. As aforementioned, the preference for $A_{\rm L} > 1$ is very mild, being the mean value of this parameter $A_{\rm L} < 1$ when CMB lensing observations are considered.

The last possibility we explore here is to consider the lensing amplitude to be an oscillatory function of the multipole ℓ, $A_{\rm L}(\ell) = A_{\rm base} + A_{\rm amp}\sin(\omega_f \ell + \phi_0)$, where $A_{\rm base}$, $A_{\rm amp}$, ω_f and ϕ_0 denote the base value, amplitude, angular frequency and initial phase of the oscillation. After confronting this model with CBS observations, we find that ω_f and ϕ_0 cannot be constrained, and the data is just sensitive to $A_{\rm base}$ and $A_{\rm amp}$. Hence, we consider a simplified oscillating model $A_{\rm L}(\ell) = A_{\rm base} + A_{\rm amp}\sin\ell$ by fixing $\omega_f = 1$ and $\phi_0 = 0$. Table IX shows the results for $A_{\rm L}$ and $A_{\rm amp}$ within the minimal ΛCDM cosmology. Notice that the data show no particular preference for $A_{\rm amp} \neq 0$. A value of $A_{\rm L} > 1$ is still favored with 2σ significance. Table X shows the equivalent but for the (μ, η) parametrization. While no strong preference for $\mu \neq 0$ and $\eta \neq 0$ is found from any of the data combinations, the mean values of μ_0 and η_0 are always larger than 1, shifting the standard growth of structure toward an *enhanced value; i.e.,* $\gamma < 0.55$. Moreover, when fixing ω_f and ϕ_0 to unity and zero, respectively, there is no any impact on the

TABLE IX. Mean values and 68% CL marginalized errors of the most relevant cosmological parameters within the ΛCDM cosmology when the lensing amplitude is an oscillatory function of the multipole ℓ, $A_{\rm L} = A_{\rm base} + A_{\rm amp}\sin\ell$. We report the results obtained by using the CMB plus lensing, CMB alone, CMB plus BAO plus supernovae Ia plus lensing and CMB plus BAO plus supernovae Ia datasets, respectively.

Parameters	CL	C	CBSL	CBS
$\Omega_b h^2$	0.02250 ± 0.00017	0.02260 ± 0.00017	0.02246 ± 0.00014	0.02253 ± 0.00014
$\Omega_c h^2$	0.1184 ± 0.0015	0.1179 ± 0.0015	0.11892 ± 0.00099	0.1188 ± 0.0010
$100\theta_{MC}$	1.04109 ± 0.00033	1.04116 ± 0.00033	1.04103 ± 0.00029	1.04103 ± 0.00030
τ	$0.0489^{+0.0085}_{-0.0077}$	0.0489 ± 0.0086	0.0490 ± 0.0079	0.0487 ± 0.0081
$\ln(10^{10}A_s)$	3.028 ± 0.018	$3.028^{+0.018}_{-0.016}$	3.030 ± 0.016	$3.030^{+0.018}_{-0.016}$
n_s	0.9695 ± 0.0049	0.9713 ± 0.0049	0.9683 ± 0.0037	0.9689 ± 0.0038
$A_{\rm base}$	1.093 ± 0.045	1.21 ± 0.17	1.085 ± 0.040	1.15 ± 0.17
$A_{\rm amp}$	0.070 ± 0.057	0.08 ± 0.47	0.071 ± 0.055	-0.04 ± 0.51
H_0	68.10 ± 0.71	68.36 ± 0.71	67.85 ± 0.45	67.94 ± 0.46
Ω_m	0.3054 ± 0.0093	0.3023 ± 0.0093	0.3086 ± 0.0059	0.3078 ± 0.0061
σ_8	0.8003 ± 0.0089	$0.7989^{+0.0094}_{-0.0084}$	0.8024 ± 0.0074	0.8023 ± 0.0078
S_8	0.807 ± 0.019	0.802 ± 0.019	0.814 ± 0.013	0.813 ± 0.014
χ^2	2786.7	2773.4	3842.4	3829.7

TABLE X. Mean values and 68% CL marginalized errors of the most relevant cosmological parameters within the growth model parametrized via μ and η, see Eq. (10), when the lensing amplitude is an oscillatory function of the multipole ℓ, $A_{\rm L} = A_{\rm base} + A_{\rm amp}\sin\ell$. We report the results obtained by using the CMB plus lensing, CMB alone, CMB plus BAO plus supernovae Ia plus lensing and CMB plus BAO plus supernovae Ia datasets, respectively.

Parameters	CL	C	CBSL	CBS
$\Omega_b h^2$	0.02250 ± 0.00017	0.02260 ± 0.00018	0.02245 ± 0.00014	0.02253 ± 0.00014
$\Omega_c h^2$	0.1186 ± 0.0015	0.1180 ± 0.0015	0.1191 ± 0.0010	0.1189 ± 0.0011
$100\theta_{MC}$	1.04107 ± 0.00032	1.04116 ± 0.00034	1.04102 ± 0.00029	1.04104 ± 0.00032
τ	$0.0494^{+0.0087}_{-0.0072}$	$0.0505^{+0.0090}_{-0.0079}$	0.0492 ± 0.0081	$0.0496^{+0.0082}_{-0.0073}$
$\ln(10^{10}A_s)$	$3.030^{+0.018}_{-0.016}$	$3.032^{+0.020}_{-0.016}$	3.030 ± 0.017	$3.032^{+0.018}_{-0.015}$
n_s	0.9687 ± 0.0048	0.9707 ± 0.0049	0.9676 ± 0.0038	0.9686 ± 0.0041
$A_{\rm base}$	$0.988^{+0.077}_{-0.087}$	1.07 ± 0.16	$0.980^{+0.072}_{-0.080}$	1.05 ± 0.18
$A_{\rm amp}$	0.041 ± 0.056	0.01 ± 0.42	0.041 ± 0.055	$0.01^{+0.63}_{-0.53}$
$\mu_0 - 1$	$0.05^{+0.24}_{-0.44}$	$0.07^{+0.26}_{-0.39}$	$0.08^{+0.25}_{-0.45}$	$0.09^{+0.26}_{-0.47}$
$\eta_0 - 1$	$0.43^{+0.58}_{-1.10}$	$0.44^{+0.62}_{-0.96}$	$0.37^{+0.59}_{-1.10}$	$0.42^{+0.71}_{-1.10}$
H_0	68.00 ± 0.68	68.33 ± 0.71	67.79 ± 0.45	67.90 ± 0.49
Ω_m	0.3067 ± 0.0091	0.3027 ± 0.0092	0.3094 ± 0.0061	0.3083 ± 0.0065
σ_8	$0.807^{+0.027}_{-0.044}$	$0.808^{+0.027}_{-0.040}$	$0.811^{+0.027}_{-0.045}$	$0.813^{+0.028}_{-0.048}$
S_8	$0.816^{+0.035}_{-0.045}$	$0.812^{+0.032}_{-0.043}$	$0.824^{+0.032}_{-0.046}$	$0.824^{+0.031}_{-0.050}$
χ^2	2786.7	2773.5	3842.4	3829.8

constraining power of the other parameters. This is still ascribed to the fact current data is only sensitive to the amplitude of the oscillation and the base value of lensing amplitude.

It is worth noting that, for all the models considered here, we find that growth index model almost has a a little smaller χ^2 than other ones for each data combination. The addition of CMB lensing data always leads to a smaller optical depth. Moreover, all the data combinations for each model gives consistent H_0 and S_8 values at the 1σ confidence level (see Tables II–X).

A final comment should be devoted to the different datasets exploited here. Notice that the CBS combination is the most conservative and ideal one, and, since, as it contains less datasets, it can avoid potential uncertainties present in the data. Also the statistical significance for $\gamma > 1$ is in general larger than when considering lensing. The combination "CBSL," being more complete, decreases the significance of the signal and also the preference for $A_L > 1$. Nevertheless, it introduces more uncertainties in the analyses, as it relies on the halofit numerical code, which has not been properly updated in the context of the different growth parametrizations considered here.

C. Signal parameter S_0 measuring cosmic growth

In the above analysis, although we have shown the constraints on different growth parametrizations from different data combinations, there is still an important and interesting issue to be addressed; i.e., what does γ or (μ_0, η_0) test at all? For example, one can easily find that CMB plus lensing gives $\gamma = 0.506 \pm 0.022$ in the growth index model, which is a 2σ signal of enhanced structure growth (see Table II) and 2σ deviation from general relativity in the (μ_0, η_0) plane (see Figs. 2 and 6). Indeed, the information of this enhanced growth can be captured and described accurately by a linear combination of μ_0 and η_0, namely by the approximate fitting formula $S_0 = \mu_0 + 0.4\eta_0$, where S_0 denotes the intercept in the μ_0 axis when $\eta_0 = 0$. Notice that S_0 is different from S_8. S_0 works in the (μ_0, η_0) plane and actually depicts the deviation from general relativity on cosmic scales. S_8 characterizes the strength of matter perturbation at a distance of $R = 8h^{-1}$ Mpc. Using the data combination of CMB temperature, polarization and lensing, we obtain the constraint $S_0 = 1.567 \pm 0.088$ at 2σ level. Note that S_0 is a derived parameter here. In Fig. 6, we have presented how S_0 serves as a signal parameter to measure the deviation from the standard growth in general relativity. It is easy to see that the S_0 parameter captures the 2σ excess very well. This means that S_0 encodes what γ or (μ_0, η_0) tests. This parameter extracts efficiently growth information that is hiding in both effective gravitational strength and anisotropic stress of cosmic species. S_0 can be generalized to test the deviation from general relativity in large scale structure observations.

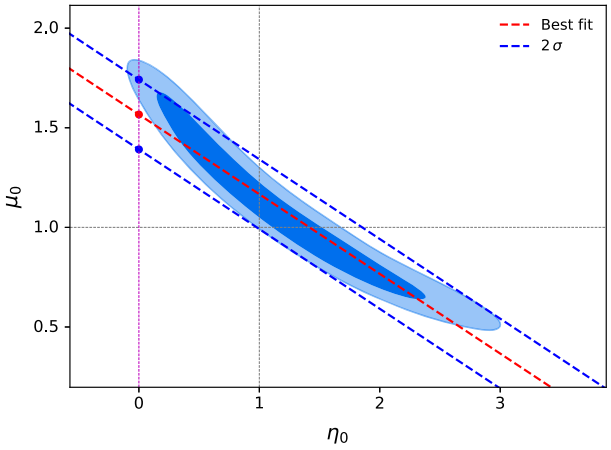

FIG. 6. S_0 acts as a signal parameter to measure the deviation from the standard cosmic growth in general relativity. The red and blue points denote the best fit value and 2σ limits of S_0, respectively. Similarly, the red and blue lines are the best fit line and 2σ boundaries when using the fitting formula $S_0 = \mu_0 + 0.4\eta_0$, respectively. The magenta dashed line corresponds to $\eta_0 = 0$, and the cross point between gray dashed lines represents general relativity. The blue contours depict the 68% and 95% confidence regions in the (η_0, μ_0) plane within the growth model parametrized via μ and η, see Eq. (10), obtained by using CMB temperature, polarization and lensing observations.

D. N-body simulations

Using the halofit model, one can easily express the nonlinear matter power spectrum as the one-halo plus the two-halo terms

$$P_{\rm nonlinear}(\gamma, k, a) = P_{1\,\rm h}(\gamma, k, a) + P_{2\,\rm h}(\gamma, k, a), \quad (11)$$

where the one-halo term is

$$P_{\rm 1h}(\gamma, k, a) = \int_0^\infty W^2(\gamma, M, k, a) n(\gamma, M, a) {\rm d}M, \quad (12)$$

and the two-halo term reads

$$P_{2\,\rm h}(\gamma, k, a) = P(\gamma, k, a)\left[\int_0^\infty W(\gamma, M, k, a) \times n(\gamma, M, a) b(\gamma, M, a) {\rm d}M\right]^2, \quad (13)$$

where $W(\gamma, M, k, a)$, $n(\gamma, M, a)$ and $b(\gamma, M, a)$ are halo density profiles, halo mass function and halo bias, respectively. It is easy to see that these three halo related quantities all depend on γ, halo mass M and a. Note that the halo density profile also depends on the scale k.

The authors of Ref. [26] claim that the linear power spectrum enters only through the variance of the matter density field in the halo mass function $n(M, a)$. In light of this setting, they derive their cosmological constraints by

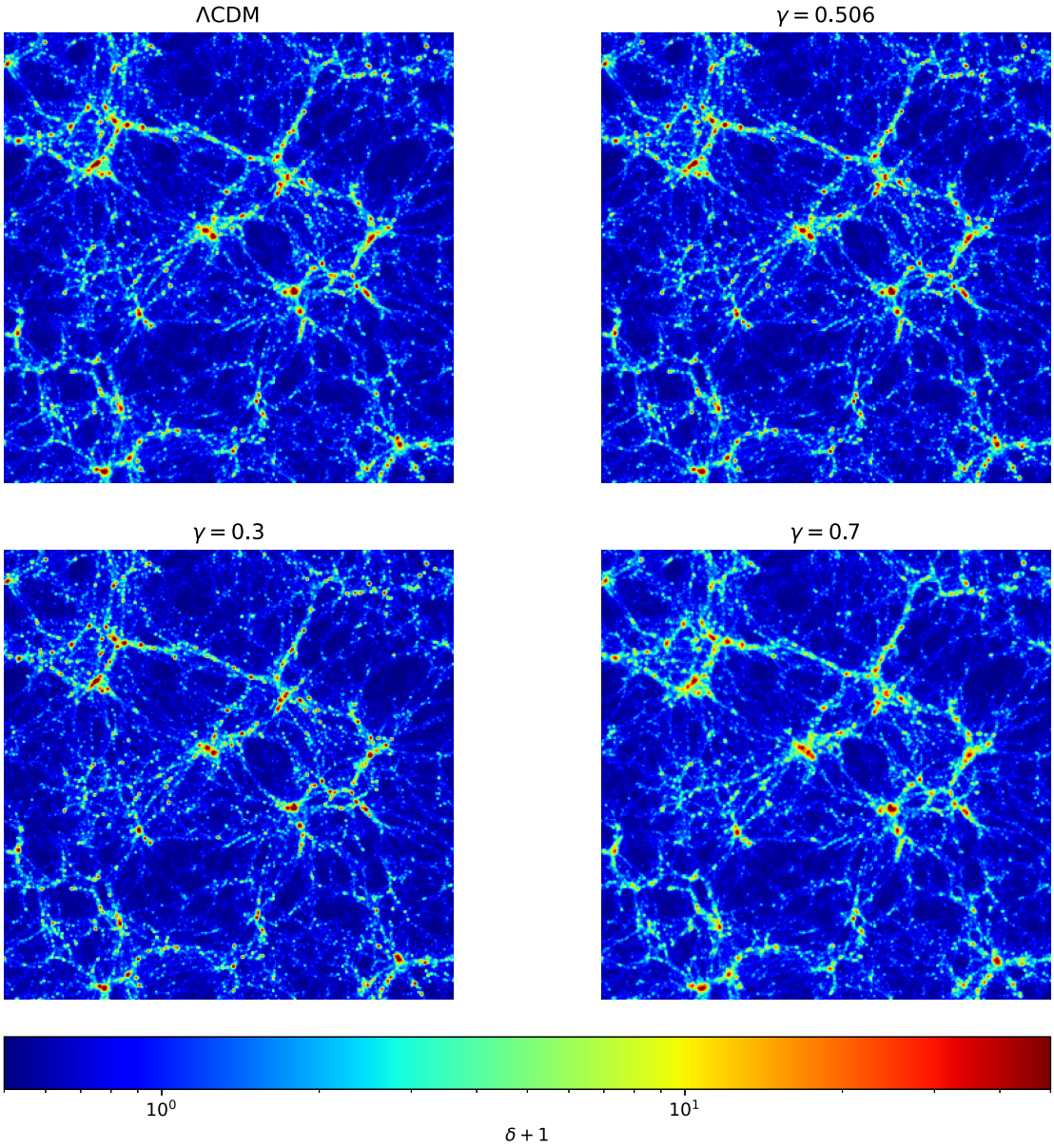

FIG. 7. Density fields of dark matter in the growth index γ model for the values $\gamma = 0.506$, 0.3 and 0.7 at redshift $z = 0$. For the case of $\gamma = 0.506$, we use the best fit of the growth index model to implement the simulation. We also depict the ΛCDM case as a reference and choose a slice of $20h^{-1}$ Mpc (i.e., $200 \times 200 \times 20h^{-3}$ Mpc^3) density field and stack it along Z axis for each model. δ denotes the overdensity of dark matter.

using weak lensing and RSD observations. However, the realistic consequence is that γ also affects both $W(\gamma, M, k, a)$ and $b(\gamma, M, a)$ in a completely nonlinear way. These effects need to be captured by numerical simulations. Therefore, based on this concern, in order to explore this issue more accurately, we implement dark matter simulations for the ΛCDM and growth index models. In general, current cosmological data is consistent with zero anisotropic stress $\eta = 0$ of relativistic species. We just need to consider ΛCDM + γ or ΛCDM + μ. However, these two models are actually equivalent when describing the structure growth of a universe. Therefore, we only need to preform forecasts for one of them. Since we are mainly studying γ, we just perform the forecast and run simulations for ΛCDM + γ. For ΛCDM, we use the best fitting values of six basic parameters from the CMB constraint as fiducial values. For the growth index model, we set the best fitting values of seven basic parameters from CMB data as fiducial values of our simulations. In seven fiducial values, $\gamma = 0.506$. Subsequently, we keep other six parameters unchanged and vary only γ to 0.3 and 0.7. In Fig. 7, we show the density fields of dark matter for the growth index model with different values. Namely, we illustrate the cases $\gamma = 0.506$ (see Table II), 0.3 and 0.7, respectively. It is easy

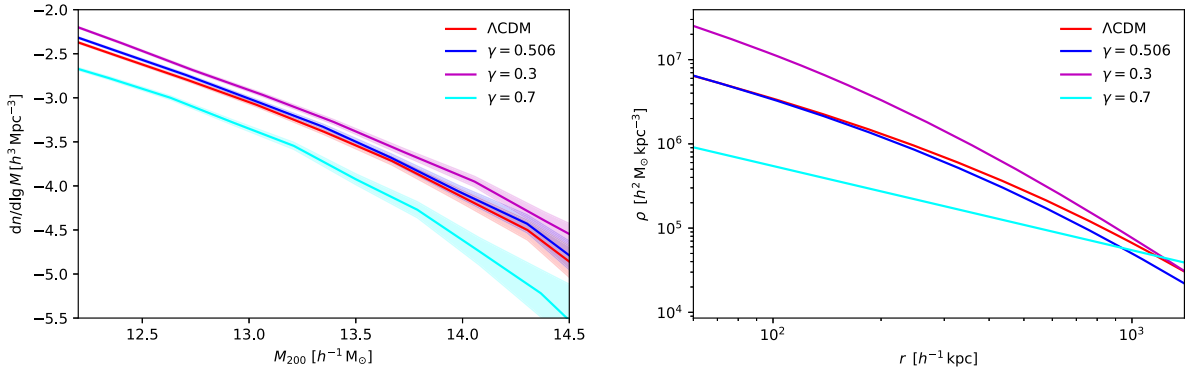

FIG. 8. Left panel: the dark matter halo mass functions in the growth index model are, respectively, shown for different values $\gamma = 0.506$, 0.3 and 0.7 at redshift $z = 0$. We also depict the halo mass function of the ΛCDM case as a reference. The shaded regions denote the Poisson errors for each model. Right panel: the dark matter halo density profiles for different models are shown.

to notice that the density fields of both ΛCDM and the best fit growth index model ($\gamma = 0.506$) are very close. However, for the case of $\gamma = 0.3$, one can observe a significant enhancement of structure growth relative to the ΛCDM case at cluster scales. Since gravitational strength is stronger than ΛCDM everywhere, a value of $\gamma = 0.3$ accelerates the process of structure formation. It is noteworthy that we do not clearly observe more small structures than in ΛCDM. For the case of $\gamma = 0.7$, the result is almost opposite to the case of $\gamma = 0.3$. We find weaker clustering of dark matter at both large and small scales and lower overdensities relative to the ΛCDM case due to weak gravitational strength: Similar structures would need more time to form when compared to the ΛCDM case.

Furthermore, we provide a quantitative analysis of different simulations. Specifically, in Fig. 8, we present the dark matter halo mass functions and halo density profiles for different values of γ in the growth index model. In light of the CMB plus lensing constraint, one can easily find that the best fit γ model predicts a little larger number of halos than ΛCDM does in the whole halo mass range. We are also interested in investigating the effects of large and small γ values on the cosmic web. In the case of $\gamma = 0.3$, an obvious enhancement of structure formation is observed relative to ΛCDM, since there are more halos generated for all the halo masses. On the contrary, fewer halos are produced in the case of $\gamma = 0.7$, which indicates that structure growth is clearly suppressed for a small γ value. In general, these statistics properties of the halo number can be seen in the density fields of dark matter (see also Fig. 7).

A representative statistical quantity describing the dark matter halo, the density profiles of dark matter halos, are also computed for the different models. Note that, for simplicity, we only study the density profile of the largest halo for each model here. We find that the best fit γ model shows the same density as ΛCDM when the radius $r < 100h^{-1}$ kpc. Nonetheless, it gives a lower density when r becomes large (say $1000h^{-1}$ kpc) and consequently predicts a lower average density of the whole halo. In the case of $\gamma = 0.3$, the halo density is clearly stronger than that in ΛCDM in the whole range of radius. Interestingly, the slope of its density profile becomes larger and reaches the same value when $r > 1000h^{-1}$ kpc relative to ΛCDM. This implies that, in a universe with an enhanced structure formation, both the average density of a halo and the halo compactness are larger than that in a ΛCDM one. In the case of $\gamma = 0.7$, the halo density is suppressed at a small radius but becomes larger than other cases starting from $r \simeq 1000h^{-1}$ kpc. This behavior is due to the fact that a weak structure growth strength decelerates the structure formation of the Universe and consequently decreases the matter accretion process of the halo. All in all, the growth index γ has an important impact on the evolution of cosmic web.

E. Forecasts for future 21 cm surveys

In the near future, there will be two type of (crucial) 21 cm large scale structure probes: 21 cm intensity mapping and HI galaxy redshift surveys [73]. The fluctuations of the brightness temperature induced by redshifted 21 cm lines trace the HI distribution and consequently detect the large scale structure of the Universe. HI galaxy redshift surveys allow us to measure the cosmic expansion history using BAO as well as the cosmic structure growth using RSD. One can constrain the matter power spectrum or correlation functions by identifying individual galaxies and confirming their redshifts and consequently determine the cosmological parameters. During the past two decades, optical galaxy redshift surveys such as SDSS [52,53,74] have achieved great success in exploring the Universe. We believe that future high-resolution HI galaxy surveys such as the Square Kilometer Array (SKA) [75,76] can give stronger constraining power on both the cosmic geometry and the growth. In this study, we focus on the forecasted constraints on the different cosmological parameters by employing

the HI galaxy redshift data from SKA Phase 2 (hereafter SKA2).

The galaxy power spectrum, in the linear regime (which is a valid approximation for the purpose of this study) for a galaxy redshift survey is expressed as [77]

$$P_g(\gamma,k,z)=[b(z)+f\xi^2]^2e^{-\frac{[k\sigma_{\rm NL}(z,\xi)]^2}{2}}P(\gamma,k,z), \quad (14)$$

where the first term depicts the so-called Kaiser effect [78], and the second one describes the "finger of God" effect due to uncorrelated velocities at small scales, which washes out the radial structure below the nonlinear velocity dispersion scale $\sigma_{\rm NL}$, $\xi\equiv\hat{k}\cdot\hat{z}$, $b(z)$ is the galaxy bias as a function of redshift z and

$$\sigma_{\rm NL}(z,\xi)=\sigma_{\rm NL}D(z)\sqrt{1+f\xi^2(2+f)}. \quad (15)$$

The quality of a galaxy redshift survey is subject to complex systematic effects. In particular, there are two main effects, namely the source evolution and bright stars as contaminants. For the former case, the luminosity function of the tracer population usually changes over redshift, which affects the detected number density of galaxies. This effect, generally characterized by the galaxy bias $b(z)$, limits the effective redshift range of a galaxy survey and make its selection function more complicated. It affects the measurement of BAO by varying the effective galaxy number density $m(z)$ to change the shot noise. It is worth noting that stars are a dominated contaminant in large optical galaxy sky surveys. Bright stars can mask galaxies behind them, when one distinguishes stars from galaxies by their color. This effect leads to a very complicated angular selection function on the sky. It is interesting that this effect is not very dangerous in the radio wavelength where SKA works, even though there are also other contaminants such as diffuse galactic synchrotron emission and some nongalaxy point sources affecting the final galaxy catalog and source-finding process; see Ref. [77] for further details.

Instead of producing mock data by implementing a full simulation, we adopt a fast and low computational cost method to forecast the uncertainties on cosmological parameters, i.e., the Fisher matrix formalism, which transforms the expected properties of signal and noise in theoretical quantities for a given survey to derive a Gaussian approximation into the underlying likelihood for a set of parameters to be measured. This method plays an important role in characterizing the ability of a given experiment to constrain the parameters of interest.

For a set of parameters $\mathbf{p}$ given the data $\mathbf{d}$, we assume that the likelihood function $\mathcal{L}$ is a Gaussian distribution and can be written as

$$\mathcal{L}(\mathbf{p}|\mathbf{d})\propto\frac{\exp\left(-\frac{1}{2}\mathbf{d}^\dagger[\mathbf{M}(\mathbf{p})]^{-1}\mathbf{d}\right)}{\sqrt{|\mathbf{M}(\mathbf{p})|}}, \quad (16)$$

where $\mathbf{M}$ is the covariance matrix of the mock data. The information of cosmological parameters seeds in the parameter vector $\mathbf{p}$. Using the fiducial values of parameters, the Fisher matrix can be constructed by the curvature of the likelihood function as

$$F_{\alpha\beta}\equiv-\left\langle\frac{\partial^2\log\mathcal{L}}{\partial p_\alpha\partial p_\beta}\right\rangle_{\mathbf{p}=\mathbf{p_0}}, \quad (17)$$

where $\mathbf{p_0}$ denotes the fiducial parameter vector.

To implement a Fisher forecast, we divide up a range of wavenumbers into bins, $\Delta_i=[k_i,k_{i+1}]$. We assign a constant value, P_i, to the power spectrum in each bin. The main physical quantities that depict a galaxy redshift survey are the sky area, S_a, and the number density of source $m(z)$. The survey volume can be defined as $V_{\rm bin}\simeq r^2(\bar{z})dr/dz\Delta z S_a$, where $r(\bar{z})=\int_0^{\bar{z}}\frac{cdz}{H(z)}$ is the radial comoving distance at the average redshift $\bar{z}$ of the survey.

For a galaxy redshift survey, the Fisher matrices read as [79,80]

$$F_{\alpha\beta}=\frac{1}{2}\int\frac{{\rm d}^3k}{(2\pi)^3}V_{\rm eff}(k)\left[\frac{\partial\ln P_T(k)}{\partial p_\alpha}\frac{\partial\ln P_T(k)}{\partial p_\beta}\right], \quad (18)$$

where P_T is the total covariance of the measured signal, which consists of the underlying signal P_S and the noise P_N. The effective volume of the experiment can be expressed as [77]

$$V_{\rm eff}(k)=V_{\rm bin}\left[\frac{m(z)P_T(k)}{1+m(z)P_T(k)}\right]^2. \quad (19)$$

Note that $V_{\rm eff}(k)$ characterizes how well different parts of Fourier space are sampled in the analysis. The signal power spectrum P_S is described by the galaxy power spectrum P_g [see Eq. (14)]. The noise power spectrum P_N can be calculated by applying Eq. (19) into the binned power spectrum, and we can obtain the uncertainties of power spectrum via the following formula [77]:

$$\left(\frac{\Delta P_i}{P_i}\right)^2=\left[\frac{1}{2}\int\frac{d^3k}{(2\pi^3)}V_{\rm eff}(k)\right]^{-1}. \quad (20)$$

For a specific galaxy survey, the Fisher matrix is computed by using Eqs. (18)–(20). Furthermore, one can obtain the errors of cosmological parameters of interest by calculating the inverse Fisher matrix.

The spectroscopic HI galaxy redshift survey SKA2 [76] will be very sensitive, and it is expected to achieve an root-mean-square (rms) flux sensitivity $S_{\rm rms}\approx 5$ μJy covering a sky area of 30000 deg^2 for 10000 hours. SKA2 aims to

TABLE XI. The expected galaxy number densities and biases for SKA2 at the redshift range of interest are shown. Note that the galaxy number densities are in units of Mpc^{-3}.

z	$m(z) \times 10^{-6}$	$b(z)$
0.23	44300	0.713
0.33	27300	0.772
0.43	16500	0.837
0.53	9890	0.907
0.63	5880	0.983
0.73	3480	1.066
0.83	2050	1.156
0.93	1210	1.254
1.03	706	1.360
1.13	411	1.475
1.23	239	1.600
1.33	139	1.735
1.43	79.9	1.882
1.53	46.0	2.041
1.63	26.4	2.214
1.73	15.1	2.402
1.81	9.66	2.566

produce a catalog of one billion HI galaxies in the redshift range $z \in (0.18, 1.84)$, which is far beyond any planned optical or near infrared experiments when $z \in (0, 1.4)$. In terms of probing BAO, the target scales are angular scales between 30 arcminutes and 4 degrees. The expected galaxy number densities and galaxy biases for SKA2 are shown in Table XI. To make a forecast, our fiducial cosmology consists of the Planck 2018 best fit cosmology ($\Omega_b h^2 = 0.02237$, $\Omega_m h^2 = 0.12$, $\ln(10^{10} A_s) = 3.044$, $\tau = 0.0544$, $n_s = 0.9649$, $\Omega_k = 0$, $H_0 = 67.36\ \mathrm{km\,s^{-1}\,Mpc^{-1}}$) and $\gamma = 0.55$.

After numerical computations, the forecasted results from SKA2 are shown in Table XII. We obtain the 1σ uncertainty $\sigma(\gamma) = 0.0083$ on the growth index γ, i.e., a 1.5% determination of the cosmic structure growth, assuming a fiducial value $\gamma = 0.55$ and therefore reducing the current errors by a factor of three. Similarly, we obtain the constraint $\sigma(H_0) = 0.19\ \mathrm{km\,s^{-1}\,Mpc^{-1}}$ relative to $H_0 = 67.36\ \mathrm{km\,s^{-1}\,Mpc^{-1}}$, which provides a 0.3% determination on H_0 and increases the accuracy of Planck's measurement by a factor of 3. Interestingly, we find the 1σ error of matter clustering amplitude $\sigma(\sigma_8) = 0.00079$, which implies a 0.098% prediction of σ_8 and improves Planck's accuracy by a factor of eight. The constraining power of SKA2 on the other six basic parameters are clearly weaker than Planck-2018 CMB data (see Table XII for details). Note that the forecast considered here is optimistic, since we assume a perfect foreground subtraction.

TABLE XII. Predicted uncertainties from SKA2 and measured errors from Planck-2018 CMB data.

Parameters	SKA2	Planck
$\sigma(\gamma)$	0.0083	0.022
$\sigma(\Omega_b h^2)$	0.0081	0.00015
$\sigma(\Omega_c h^2)$	0.0081	0.0012
$\sigma(100\theta_{MC})$	0.02741	0.00031
$\sigma(\tau)$	0.0083	0.0073
$\sigma(\ln 10^{10} A_s)$	0.2417	0.014
$\sigma(n_s)$	0.1184	0.0042
$\sigma(H_0)$	0.19	0.54
$\sigma(\sigma_8)$	0.00079	0.006

IV. DISCUSSIONS AND CONCLUSIONS

A number of cosmological tensions suggest the necessity of testing the canonical cosmological ΛCDM paradigm at a variety of epochs in the Universe's evolution. Some of these tensions may require one to modify the standard model of structure formation in our universe. It is therefore timely to evaluate whether current cosmological observations point to a departure from the standard growth picture. In the simplest parametrization, the growth of structure is simply modeled via a single parameter γ, with $f \equiv d\delta/d\ln a \equiv \Omega_m(a)^\gamma$ and $\gamma \simeq 0.55$ in the standard ΛCDM case. A recent analysis has suggested a lower structure growth which in turns implies $\gamma > 0.55$. Here we further explore this issue extending the analysis to other possible growth parametrizations. In all the cases, for the set of cosmological observations considered here, we obtain *a higher growth of structure*, characterized by $\gamma < 0.55$. Such a preference reaches the 3σ significance using cosmic microwave background observations (excluding lensing, see below), supernova Ia and baryon acoustic oscillation measurements, while the addition of cosmic microwave background lensing data relaxes such a preference to the 2σ level, since a larger lensing effect can always be compensated with a smaller structure growth, or, equivalently, with $\gamma > 0.55$. Nevertheless, when considering the very same datasets that those previously considered in the literature regardless the validity of the analyses based on assumptions on the halo model [26], we are also able to reproduce previous claims. However, the most conservative data combination considered throughout our analyses and the self-consistent growth parametrization employed here make the robust prediction of *an enhanced structure growth*, rather than a suppressed one. We have also included the lensing amplitude $A_{\rm L}$ as a free parameter in our data analyses, showing that the preference for $A_{\rm L} > 1$ observed within the canonical ΛCDM paradigm still remains, except for some particular parametrizations when lensing observations are included. There is a clear very large degeneracy between the lensing amplitude and the growth rate index γ, as a larger value of $A_{\rm L}$, implying more lensing can always be compensated by $\gamma > 0.55$, reducing structure formation and also CMB lensing (to compensate for the effect of a larger $A_{\rm L}$). We also do not find any significant preference for an oscillatory dependence of $A_{\rm L} \to A_{\rm L} + A_m \sin \ell$. To further

reassess the effects of a nonstandard growth index, we have computed by means of N-body simulations the dark matter density field, the dark matter halo mass functions and the halo density profiles for different values of γ in the growth index model. For $\gamma < 0.55$, a large number of halos and a stronger dark matter halo density profile are found, with respect to the canonical ΛCDM case. A Fisher forecast for LCDM + γ was also performed to study the future sensitivity of the SKA HI galaxy redshift data to the growth index γ, showing that the current errors could be reduced by a factor of 3, testing further the validity of the standard model of structure formation.

ACKNOWLEDGMENTS

We warmly thank the referee for helping improve the manuscript. This work has been supported by the Spanish MCIN/AEI/10.13039/501100011033 Grant No. PID2020–113644GB-I00 and by the European ITN project HIDDeN (H2020-MSCA-ITN-2019/860881-HIDDeN) and SE project ASYMMETRY (HORIZON-MSCA-2021-SE-01/101086085-ASYMMETRY) and well as by the Generalitat Valenciana grants PROMETEO/2019/083 and CIPROM/2022/69. D. W. is supported by the CDEIGENT Project of Consejo Superior de Investigaciones Científicas (CSIC).

[1] A. G. Riess, L. Breuval, W. Yuan, S. Casertano, L. M. Macri, D. Scolnic, T. Cantat-Gaudin, R. I. Anderson, and M. C. Reyes, Astrophys. J. **938**, 36 (2022).
[2] N. Aghanim *et al.* (Planck Collaboration), Astron. Astrophys. **641**, A6 (2020); **652**, C4(E) (2021).
[3] A. G. Riess *et al.*, Astrophys. J. Lett. **934**, L7 (2022).
[4] W. L. Freedman, Astrophys. J. **919**, 16 (2021).
[5] W. L. Freedman *et al.*, Astrophys. J. **882**, 34 (2019).
[6] K. C. Wong *et al.*, Mon. Not. R. Astron. Soc. **465**, 4895 (2017).
[7] S. Birrer and T. Treu, Astron. Astrophys. **649**, A61 (2021).
[8] L. F. Secco *et al.* (DES Collaboration), Phys. Rev. D **105**, 023515 (2022).
[9] T. M. C. Abbott *et al.* (DES Collaboration), Phys. Rev. D **107**, 083504 (2023).
[10] https://www.darkenergysurvey.org.
[11] C. Heymans *et al.*, Astron. Astrophys. **646**, A140 (2021).
[12] T. Tröster *et al.* (KiDS Collaboration), Astron. Astrophys. **649**, A88 (2021).
[13] https://kids.strw.leidenuniv.nl.
[14] S. A. Adil, O. Akarsu, M. Malekjani, E. O. Colgáin, S. Pourojaghi, A. A. Sen, and M. M. Sheikh-Jabbari, Mon. Not. R. Astron. Soc. **528**, L20 (2023).
[15] T. M. C. Abbott *et al.* (Kilo-Degree Survey and Dark Energy Survey Collaborations), Open J. Astrophys. **6** (2023), 10.21105/astro.2305.17173.
[16] P. Motloch and W. Hu, Phys. Rev. D **97**, 103536 (2018).
[17] E. Calabrese, A. Slosar, A. Melchiorri, G. F. Smoot, and O. Zahn, Phys. Rev. D **77**, 123531 (2008).
[18] S. Aiola *et al.* (ACT Collaboration), J. Cosmol. Astropart. Phys. 12 (2020) 047.
[19] L.-M. Wang and P. J. Steinhardt, Astrophys. J. **508**, 483 (1998).
[20] E. V. Linder, Phys. Rev. D **72**, 043529 (2005).
[21] E. V. Linder and R. N. Cahn, Astropart. Phys. **28**, 481 (2007).
[22] See Refs. [23–25] for other scenarios.
[23] M. K. Sharma and S. Sur, Phys. Dark Universe **40**, 101192 (2023).
[24] M. K. Sharma and S. Sur, Int. J. Mod. Phys. D **31**, 2250017 (2022).
[25] M. K. Sharma and S. Sur, arXiv:2102.01525.
[26] N.-M. Nguyen, D. Huterer, and Y. Wen, Phys. Rev. Lett. **131**, 111001 (2023).
[27] S. Basilakos and F. K. Anagnostopoulos, Eur. Phys. J. C **80**, 212 (2020).
[28] Z. Sakr, Universe **9**, 366 (2023).
[29] G.-B. Zhao, L. Pogosian, A. Silvestri, and J. Zylberberg, Phys. Rev. D **79**, 083513 (2009).
[30] L. Pogosian, A. Silvestri, K. Koyama, and G.-B. Zhao, Phys. Rev. D **81**, 104023 (2010).
[31] S. Casas, M. Kunz, M. Martinelli, and V. Pettorino, Phys. Dark Universe **18**, 73 (2017).
[32] A. Hojjati, L. Pogosian, and G.-B. Zhao, J. Cosmol. Astropart. Phys. 08 (2011) 005.
[33] A. Zucca, L. Pogosian, A. Silvestri, and G.-B. Zhao, J. Cosmol. Astropart. Phys. 05 (2019) 001.
[34] Z. Wang, S. H. Mirpoorian, L. Pogosian, A. Silvestri, and G.-B. Zhao, J. Cosmol. Astropart. Phys. 08 (2023) 038.
[35] A. Lewis, A. Challinor, and A. Lasenby, Astrophys. J. **538**, 473 (2000).
[36] A. Lewis and S. Bridle, Phys. Rev. D **66**, 103511 (2002).
[37] A. Lewis, arXiv:1910.13970.
[38] A. Gelman and D. B. Rubin, Stat. Sci. **7**, 457 (1992).
[39] R. E. Smith, J. A. Peacock, A. Jenkins, S. D. M. White, C. S. Frenk, F. R. Pearce, P. A. Thomas, G. Efstathiou, and H. M. P. Couchmann (VIRGO Consortium Collaboration), Mon. Not. R. Astron. Soc. **341**, 1311 (2003).
[40] S. Bird, M. Viel, and M. G. Haehnelt, Mon. Not. R. Astron. Soc. **420**, 2551 (2012).
[41] R. Takahashi, M. Sato, T. Nishimichi, A. Taruya, and M. Oguri, Astrophys. J. **761**, 152 (2012).
[42] V. Springel, Mon. Not. R. Astron. Soc. **364**, 1105 (2005).
[43] M. Crocce, S. Pueblas, and R. Scoccimarro, Mon. Not. R. Astron. Soc. **373**, 369 (2006).
[44] S. R. Knollmann and A. Knebe, Astrophys. J. Suppl. Ser. **182**, 608 (2009).
[45] N. Aghanim *et al.* (Planck Collaboration), Astron. Astrophys. **641**, A5 (2020).
[46] N. Aghanim *et al.* (Planck Collaboration), Astron. Astrophys. **641**, A1 (2020).
[47] https://pla.esac.esa.int.

[48] N. Aghanim *et al.* (Planck Collaboration), Astron. Astrophys. **641**, A8 (2020).
[49] F. Beutler, C. Blake, M. Colless, D. H. Jones, L. Staveley-Smith, L. Campbell, Q. Parker, W. Saunders, and F. Watson, Mon. Not. R. Astron. Soc. **416**, 3017 (2011).
[50] A. J. Ross, L. Samushia, C. Howlett, W. J. Percival, A. Burden, and M. Manera, Mon. Not. R. Astron. Soc. **449**, 835 (2015).
[51] S. Alam *et al.* (BOSS Collaboration), Mon. Not. R. Astron. Soc. **470**, 2617 (2017).
[52] S. Alam *et al.* (eBOSS Collaboration), Phys. Rev. D **103**, 083533 (2021).
[53] A. J. Ross *et al.*, Mon. Not. R. Astron. Soc. **498**, 2354 (2020).
[54] D. Scolnic *et al.*, Astrophys. J. **938**, 113 (2022).
[55] D. M. Scolnic *et al.* (Pan-STARRS1 Collaboration), Astrophys. J. **859**, 101 (2018).
[56] R. Trotta, Mon. Not. R. Astron. Soc. **378**, 72 (2007).
[57] T. M. C. Abbott *et al.* (DES Collaboration), Phys. Rev. D **98**, 043526 (2018).
[58] J. Prat *et al.* (DES Collaboration), Phys. Rev. D **98**, 042005 (2018).
[59] J. Elvin-Poole *et al.* (DES Collaboration), Phys. Rev. D **98**, 042006 (2018).
[60] M. A. Troxel *et al.* (DES Collaboration), Phys. Rev. D **98**, 043528 (2018).
[61] T. M. C. Abbott *et al.* (DES Collaboration), Phys. Rev. D **99**, 123505 (2019).
[62] K. Said, M. Colless, C. Magoulas, J. R. Lucey, and M. J. Hudson, Mon. Not. R. Astron. Soc. **497**, 1275 (2020).
[63] F. Beutler, C. Blake, M. Colless, D. H. Jones, L. Staveley-Smith, G. B. Poole, L. Campbell, Q. Parker, W. Saunders, and F. Watson, Mon. Not. R. Astron. Soc. **423**, 3430 (2012).
[64] D. Huterer, D. Shafer, D. Scolnic, and F. Schmidt, J. Cosmol. Astropart. Phys. 05 (2017) 015.
[65] S. S. Boruah, M. J. Hudson, and G. Lavaux, Mon. Not. R. Astron. Soc. **498**, 2703 (2020).
[66] R. J. Turner, C. Blake, and R. Ruggeri, Mon. Not. R. Astron. Soc. **518**, 2436 (2022).
[67] C. Blake *et al.*, Mon. Not. R. Astron. Soc. **415**, 2876 (2011).
[68] C. Blake *et al.*, Mon. Not. R. Astron. Soc. **436**, 3089 (2013).
[69] C. Howlett, A. Ross, L. Samushia, W. Percival, and M. Manera, Mon. Not. R. Astron. Soc. **449**, 848 (2015).
[70] T. Okumura *et al.*, Publ. Astron. Soc. Jpn. **68**, 38 (2016).
[71] A. Pezzotta *et al.*, Astron. Astrophys. **604**, A33 (2017).
[72] S. Nesseris, G. Pantazis, and L. Perivolaropoulos, Phys. Rev. D **96**, 023542 (2017).
[73] R. Ansari, in *56th Rencontres de Moriond on Cosmology* (2022), arXiv:2203.17039.
[74] https://www.sdss4.org.
[75] https://www.skao.int.
[76] M. G. Santos *et al.*, Proc. Sci. AASKA14 (**2015**) 019 [arXiv:1501.03989].
[77] P. Bull, P. G. Ferreira, P. Patel, and M. G. Santos, Astrophys. J. **803**, 21 (2015).
[78] N. Kaiser, Mon. Not. R. Astron. Soc. **227**, 1 (1987).
[79] H.-J. Seo and D. J. Eisenstein, Astrophys. J. **598**, 720 (2003).
[80] H.-J. Seo and D. J. Eisenstein, Astrophys. J. **665**, 14 (2007).